ESC European Society of Cardiology

European Heart Journal (2023) **44**, 885–898
https://doi.org/10.1093/eurheartj/ehac818

TRANSLATIONAL RESEARCH
Valvular heart disease

Sortilin enhances fibrosis and calcification in aortic valve disease by inducing interstitial cell heterogeneity

Farwah Iqbal [1†], Florian Schlotter [2,3†], Dakota Becker-Greene [1†], Adrien Lupieri [1], Claudia Goettsch [2,4], Joshua D. Hutcheson[2,5], Maximillian A. Rogers [2], Shinsuke Itoh [2], Arda Halu [2,6], Lang Ho Lee[2], Mark C. Blaser [2], Andrew K. Mlynarchik[2], Sumihiko Hagita[2], Shiori Kuraoka[2], Hao Yu Chen[7], James C. Engert[7], Livia S.A. Passos [1], Prabhash K. Jha[1], Eric A. Osborn [8], Farouc A. Jaffer [9], Simon C. Body [10], Simon C. Robson [11], George Thanassoulis[7], Masanori Aikawa [1,2,6], Sasha A. Singh [2], Abhijeet R. Sonawane [1,2], and Elena Aikawa [1,2]*

[1]Center for Excellence in Vascular Biology, Division of Cardiovascular Medicine, Brigham and Women's Hospital, Harvard Medical School, Boston, MA, USA; [2]Center for Interdisciplinary Cardiovascular Sciences, Division of Cardiovascular Medicine, Brigham and Women's Hospital, Harvard Medical School, Boston, MA, USA; [3]Department of Cardiology, Heart Center Leipzig at Leipzig University, Leipzig, Germany; [4]Department of Internal Medicine I, Cardiology, Medical Faculty, RWTH Aachen University, Aachen, Germany; [5]Department of Biomedical Engineering, Florida International University, Miami, FL, USA; [6]Channing Division of Network Medicine, Brigham and Women's Hospital, Harvard Medical School, Boston, MA, USA; [7]Department of Medicine, McGill University, Montreal, Canada; [8]Division of Cardiovascular Medicine, Beth Israel Deaconess Medical Center, Harvard Medical School, Boston, MA, USA; [9]Cardiovascular Research Center, Division of Cardiology, Massachusetts General Hospital, Harvard Medical School, Boston, MA, USA; [10]Department of Anesthesiology, Boston University School of Medicine, Boston, MA, USA; and [11]Center for Inflammation Research, Department of Anesthesia, BIDMC, Harvard Medical School, Boston, MA, USA

Received 28 March 2022; revised 29 November 2022; accepted 22 December 2022; online publish-ahead-of-print 20 January 2023

See the editorial comment for this article 'Have we found the missing link between inflammation, fibrosis, and calcification in calcific aortic valve disease?', by M. Martin *et al.*, https://doi.org/10.1093/eurheartj/ehac787.

Abstract

Aims Calcific aortic valve disease (CAVD) is the most common valve disease, which consists of a chronic interplay of inflammation, fibrosis, and calcification. In this study, sortilin (SORT1) was identified as a novel key player in the pathophysiology of CAVD, and its role in the transformation of valvular interstitial cells (VICs) into pathological phenotypes is explored.

Methods and results An aortic valve (AV) wire injury (AVWI) mouse model with sortilin deficiency was used to determine the effects of sortilin on AV stenosis, fibrosis, and calcification. *In vitro* experiments employed human primary VICs cultured in osteogenic conditions for 7, 14, and 21 days; and processed for imaging, proteomics, and transcriptomics including single-cell RNA-sequencing (scRNA-seq). The AVWI mouse model showed reduced AV fibrosis, calcification, and stenosis in sortilin-deficient mice vs. littermate controls. Protein studies identified the transition of human VICs into a myofibroblast-like phenotype mediated by sortilin. Sortilin loss-of-function decreased *in vitro* VIC calcification. ScRNA-seq identified 12 differentially expressed cell clusters in human VIC samples, where a novel combined inflammatory myofibroblastic-osteogenic VIC (IMO-VIC) phenotype was detected with increased expression of SORT1, COL1A1, WNT5A, IL-6, and serum amyloid A1. VICs sequenced with sortilin deficiency showed decreased IMO-VIC phenotype.

Conclusion Sortilin promotes CAVD by mediating valvular fibrosis and calcification, and a newly identified phenotype (IMO-VIC). This is the first study to examine the role of sortilin in valvular calcification and it may render it a therapeutic target to inhibit IMO-VIC emergence by simultaneously reducing inflammation, fibrosis, and calcification, the three key pathological processes underlying CAVD.

* Corresponding author. Tel: +1 617 730 7755, Fax: +1 617 730 7791, Email: eaikawa@bwh.harvard.edu
† These authors contributed equally to this work.

Structured Graphical Abstract

Key Question

What is the role of sortilin in aortic valve fibrosis and calcification in calcific aortic valve disease (CAVD)? How heterogenous are valvular interstitial cells (VIC) and is there a disease driving cell population(s) in CAVD?

Key Finding

An aortic valve injury mouse model showed decreased aortic valve fibrosis and calcification with attenuated sortilin expression. A novel combined inflammatory myofibroblastic-osteogenic VIC population was identified in human CAVD samples.

Take Home Message

In vivo wire injury mouse model and in vitro osteogenic cultures using human cultured VIC reveal the role of sortilin in driving fibrosis and calcification in CAVD. Targeting newly identified VIC populations with myofibroblastic-osteogenic properties is a promising strategy to slow CAVD progression.

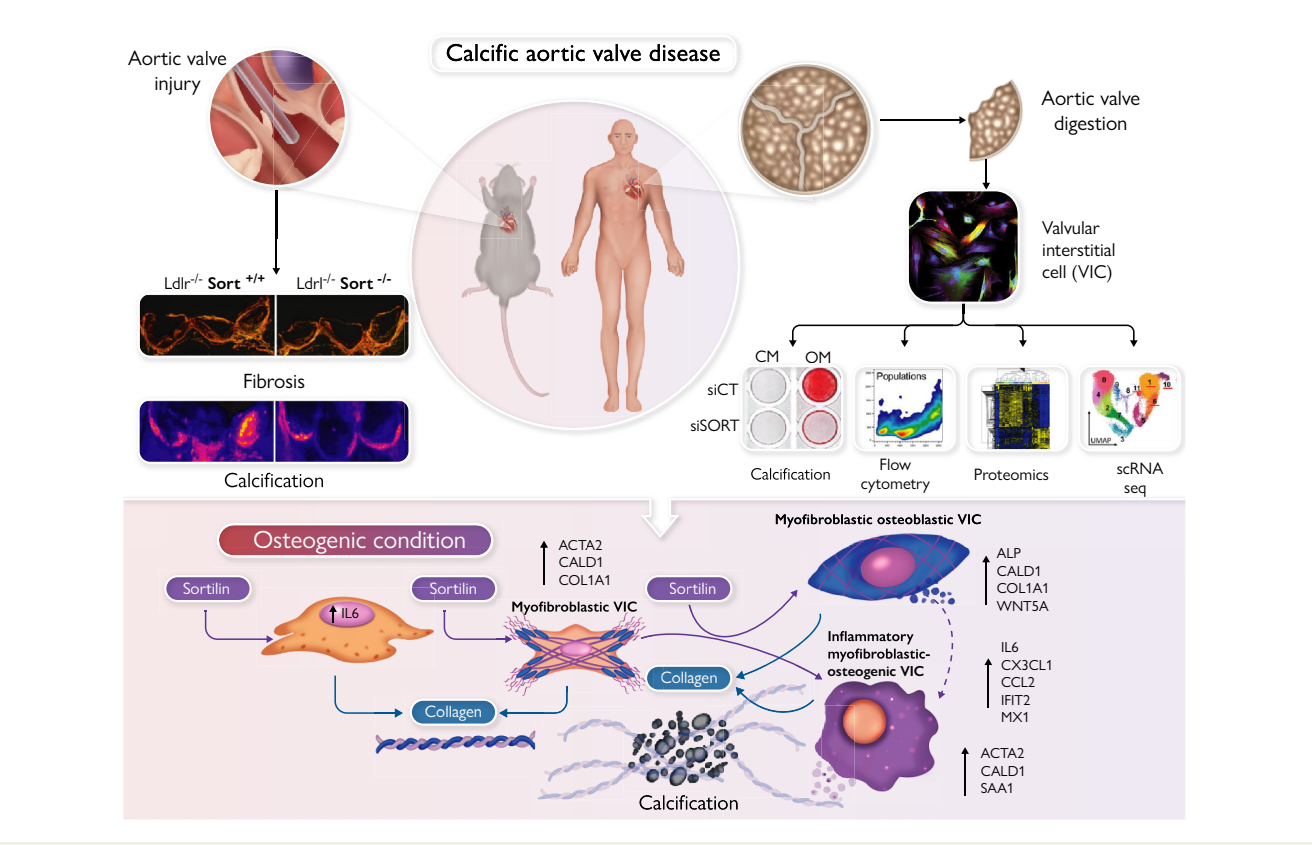

Multi-omic approach to identify the role of sortilin in mediating fibrosis and calcification in calcific aortic valve disease (CAVD). Aortic valve (AV) wire injury in sortilin wild-type (Sort1$^{+/+}$) and deficient mice (Sort1$^{-/-}$) showed decreased collagen deposition and calcification in mouse AVs. Valvular interstitial cells (VICs) were collected from human CAVD tissue and cultured in osteogenic conditions. VICs collected at varying time points of culture (Days 7, 14, and 21) were processed for flow cytometry, proteomics, and single-cell RNA-sequencing (scRNA-seq). Multiomics data identified increased sortilin expression following the osteogenic culture of VICs. Protein analysis and scRNA-seq identified increased expression of WNT5a, MAPK, YAP, and IL-6 regulated by the expression of sortilin. ScRNA-seq identified a transitionary VIC subpopulation with an activated myofibroblast phenotype that later transitioned into a combined myofibroblast and osteogenic phenotype. ScRNA-seq data identified an inflammatory myofibroblastic-osteogenic VIC (IMO-VIC) subpopulation that may be a key player in the pathogenesis of CAVD under the regulation of sortilin.

Keywords Aortic stenosis • Calcification • Fibrosis • Inflammation • Single-cell RNA-sequencing • Sortilin

Translational Perspective

- Sortilin was identified as a key mediator of calcific aortic valve disease (CAVD) with adverse effects on three key cornerstones of CAVD pathogenesis—inflammation, fibrosis, and calcification.
- Single-cell RNA-sequencing identified a novel pathogenic human aortic valve interstitial cell subset with combined inflammatory myofibroblastic-osteogenic properties.
- Targeting this valvular interstitial cell subpopulation through sortilin inhibition may translate into a promising mechanism to halt CAVD progression.

Introduction

Calcific aortic valve disease (CAVD) leading to aortic stenosis (AS) is the most prevalent valve disease necessitating clinical intervention.[1] The pathophysiology is primarily characterized by the accumulation and activation of various cell types that promote leaflet fibrosis and calcification, resulting in the obstruction of left ventricular outflow.[2–4] The current paradigm suggests that valvular interstitial cells (VICs) comprise the majority of the aortic valve (AV) and are typically quiescent in healthy AVs. Under pathological conditions VICs transition into activated myofibroblasts, which secrete excessive extracellular matrix (ECM), including collagen, leading to AV stiffening.[5] In addition, VICs with calcifying properties express osteogenic markers [RUNX2, osteopontin, osteocalcin, alkaline phosphatase (ALP)] and deposit bone-like mineralized material. An emerging hypothesis suggests that VICs are a more heterogeneous population than previously thought; yet the signals that trigger VIC activation and differentiation remain unclear.[6] Despite a few potential molecular targets,[7,8] there are currently no screening tests to detect CAVD in high-risk patients and anti-calcification drugs are not available.[9] There is a need to identify early-stage modulators of CAVD to prevent disease progression and avert or delay AV intervention.[10]

Sortilin, a type I membrane glycoprotein encoded by the SORT1 gene, has protein-sorting functions and is known to regulate lipid metabolism, inflammation, and vascular calcification.[11,12] Global deletion of SORT1 reduces levels of very low-density lipoproteins from the liver[13] and in atherosclerotic mice,[14,15] which are associated with the onset of AV calcification.[16] Sortilin is also associated with calcified regions in patients' atheroma with chronic renal disease,[17] and genetic deletion of *Apoe/Sort1* reduces vascular calcification.[17] Moreover, mechanistic studies demonstrated that sortilin promotes vascular calcification by shuttling ALP into smooth muscle cell (SMC)-secreted extracellular vesicles, but its role in valvular calcification has not been characterized.[17] Of note, despite sharing the same endpoint of calcific mineral accumulation, atherosclerosis/vascular calcification and CAVD/valvular calcification are vastly different in a number of features, including predominant cell types, biochemical tissue stresses, ECM composition and tissue penetrance.[18,19] The role of sortilin in VIC-mediated calcification in CAVD has not been investigated; therefore, understanding its role in mediating valvular fibrosis and calcification may render it a novel target in CAVD.

This present study aimed to integrate multi-omic approaches and systems biology to build on the understanding of CAVD pathogenesis by identifying VIC heterogeneity and potential VIC disease-driving sub-populations. Mechanistic studies were conducted to elucidate the role of sortilin in VIC-mediated fibrosis and calcification. Single-cell RNA-sequencing (scRNA-seq) studies identified the emergence of a novel VIC subpopulation with combined inflammatory myofibroblastic-osteogenic phenotypes (IMO-VICs), which may be a target disease-driver population in CAVD.

Methods

Detailed methods are presented in the Supplementary material online, *Methods*. The data that support the findings of this study are available from the corresponding author, [E.A], upon reasonable request.

Genetic associations in human cohorts

All analyses were approved by the appropriate review boards at Kaiser Permanente Northern California and the McGill University Health Centre (2015-1292). The UK Biobank was approved by the North-West Multi-Center Research Ethics Committee (11/NW/0382) as a research tissue bank. Analyses performed in the UK Biobank in application 41025 were approved by the internal review board at the McGill University Health Centre (2015-1292).

In the Genetic Epidemiology Research on Adult Health and Aging (GERA) cohort (55 180 European-ancestry participants; 3469 cases) and the UK Biobank (247 417 White British participants; 3443 cases), the association with prevalent AS of variants within 50 kb of *SORT1* transcription (GRCh37 109 802 197–109 990 540) was assessed using logistic regression. The models were adjusted for age, age squared, sex, and 10 principal components in the GERA cohort, and age, age squared, sex, genotype batch, and 20 principal components in the UK Biobank (see Supplementary material online, *Methods*).

In vivo analyses

All animal experiments were performed in compliance with the Institutional Animal Care and Use Committee at Beth Israel Deaconess Medical Center under animal protocol #010-2016 (Boston, MA, USA). Female and male low-density lipoprotein receptor-deficient ($Ldlr^{-/-}$) and $sortilin^{-/-}$ mice, on a high-fat, high-cholesterol diet (HF/HC), underwent AV wire injury (AVWI) ($n = 10–12$). Echocardiography was performed to evaluate AV function, while multiphoton and confocal imaging was utilized to quantify AV fibrosis and microcalcification.

In vitro experiments including valvular interstitial cell loss-of-function studies, proteomics, and single-cell RNA-sequencing

Human VICs were isolated from AV tissue, collected from patients undergoing AV replacement procedures (see Supplementary material online, *Methods* and *Table 1*). The study protocol was approved by the Institutional Review Board and Human Research Committee at Brigham and Women's Hospital (2011P001703) including 10 donors. VICs were expanded in normal growth media (GM) composed of DMEM supplemented with 10% FBS and 1% P/S and then cultured in control media (CM), DMEM with 5% FBS and 1% P/S; or osteogenic media (OM), DMEM with 5% FBS, 1% P/S, 10 nM dexamethasone, 10 mM β-glycerol phosphate, and 100 mM L-ascorbate phosphate for 21 days (see Supplementary material online, *Methods*). Loss-of-function studies used small interfering RNA (siRNA) encapsulated in a lipid transfection agent to attenuate sortilin expression. VICs were processed for flow cytometry, quantitative polymerase chain reaction (qPCR), and western blot for VIC characterization at days 14 and 21 of culture (see Supplementary material online, *Methods*). VICs were lysed at day 14 to quantify ALP activity and Alizarin red density to quantify *in vitro*

Table 1 Baseline clinical and echocardiographic parameters of the tissue donors

Age, years	58 ± 15
Female sex, *n* (%)	2 (17)
Diabetes, *n* (%)	1 (9)
Arterial hypertension, *n* (%)	7 (58)
Hyperlipidaemia, *n* (%)	7 (58)
Serum creatinine (mg/dL)	0.96 ± 0.21
Smoking, *n* (%)	8 (67)
Left ventricular ejection fraction (%)	60 ± 8
Aortic valve area (cm^2)	0.95 ± 0.15
Aortic valve peak gradient (mmHg)	64 ± 15
Aortic valve mean gradient (mmHg)	41 ± 7
Previous percutaneous coronary intervention (PCI), *n* (%)	1 (9)
Previous coronary artery bypass graft (CABG), *n* (%)	2 (17)
Previous myocardial infarction (MI), *n* (%)	1 (9)
Statin, *n* (%)	6 (50)
Angiotensin-converting enzyme (ACE) or Angiotensin II receptor inhibitor, *n* (%)	5 (42)
Bisphosphonate, *n* (%)	0

calcification. VICs were co-cultured with p38 MAPK inhibitor for 14 days and processed for qPCR. Liquid chromatography–tandem mass spectrometry for proteomics used the Thermo Fisher Oribitrap Fusion Lumos mass spectrometer with a Nanospray FLEX ion source and coupled to an Easy-nlC1000 HPLC pump (see Supplementary material online, *Methods*). Mass spectrometry data were analysed using Proteome Discoverer Package (Version 2.2, Thermo Fisher Scientific), and subsequent statistical analyses using Qlucore Omics Explorer. Pathway enrichment analysis was performed using ConsensusPathDB.[20] Pathway networks were constructed using Python 3.8.1 and network visualizations were done in Gephi v0.9.2. scRNA-seq was conducted using the 10× Genomics platform. After cDNA library sequencing (Illumina NovaSeq), raw data were analysed using Cell Ranger v3.1, Loupe v4.0, Seurat v4.0, R studio v.1.41717, and Excel.

Statistical analysis

Two group comparisons were performed by *t*-test or Mann–Whitney *U* test for non-parametric data. Data analysis on multiple groups was conducted by ANOVA or Kruskal–Wallis test and Bonferroni or Dunn's multiple comparisons test (GraphPad). Normal distribution of data was evaluated by Kolmogorov–Smirnov test. *P*-values <0.05 were considered statistically significant. The '±' indicates standard error of the mean. For proteomics, multigroup comparisons were made using two-way ANOVA filtering for *P*-values <0.05 and false discovery rates <0.05 (Qlucore Omics 2.2, Qlucore Sweden). Hierarchical clustering for protein profiling was done using Qlucore. scRNA-seq data analysis was performed using Seurat 4.0.[21,22] implemented in R studio. Features detected in more than five cells were selected. Sparse data matrix from the 10× genomics platform was read using '*Read10x*' function for all samples, and combined into one Seurat object using '*merge*' function.

Results

Genetic association of SORT1 with aortic stenosis

In the GERA and UK Biobank cohorts, totalling 302,597 participants (6912 cases), a meta-analysis was performed for the association with AS of 555 variants within 50 kb of *SORT1* (*Figure 1A*). Eleven variants were strongly associated with disease ($P \leq 1 \times 10^{-5}$), but likely comprised one independent signal (all $r^2 \geq 0.60$) (*Table 2*). Each copy of the lead variant rs599839-A conferred 11% increased odds of AS [odds ratio per risk allele, 1.11; 95% confidence interval (CI), 1.07–1.16; $P = 1.2 \times 10^{-6}$]. While rs599839 was predicted to be benign [combined annotation dependent depletion (CADD) *C*-score = 0.03], three variants in linkage disequilibrium had CADD *C*-scores ≥ 11.0, suggesting possible deleterious effects (*Table 2*). In the UK Biobank, where low-density lipoprotein cholesterol (LDL-C) had been measured, the association of these 11 variants with AS persisted following further adjustment for LDL-C and cholesterol-lowering medication use, with only modest attenuation of estimated effects (*Table 2*). Additional sensitivity analyses were performed including (i) exclusion of all individuals ($n = 69\,861$) on lipid-lowering medication at baseline and (ii) statistical adjustment using imputing LDL-C values for those on lipid-lowering medications (imputed LDL-C = LDL-C × 1.36). Both sensitivity analyses were consistent with the primary analysis (see Supplementary material online, *Figure S1*). Subsequent expansion of the meta-analysed region to include 206 upstream variants within 50 kb of the *CELSR2-PSRC1-SORT1* locus did not identify additional variants associated with AS ($P \geq 3.3 \times 10^{-4}$).

Sortilin deficiency attenuates aortic stenosis development and reduces aortic valve fibrosis and calcification in a mouse model of calcific aortic valve disease

Our group previously established $Ldlr^{-/-}/Sort1^{-/-}$ mice to identify the role of sortilin in mediating vascular calcification.[17] In this present study, we introduced AVWI to translate CAVD in a mouse model and to explore the role of sortilin in CAVD (see Supplementary material online, *Figure S2A–C*). $Ldlr^{-/-}/Sort1^{+/+}$ and $Ldlr^{-/-}/Sort^{-/-}$ littermates were fed a HF/HC diet and underwent AVWI, sham procedure (ligation of carotid artery) or no procedure (NP) ($n \geq 10$). Animal groups were followed to 16 weeks post AVWI (*Figure 1B*). AV leaflets from $Ldlr^{-/-}/Sort1^{+/+}$ mice had significantly higher stiffness relative to $Ldlr^{-/-}/Sort1^{-/-}$ mice ($P < 0.01$), assessed by atomic force microscopy (see Supplementary material online, *Figure S2D*). Color flow Doppler of AVs at 16 weeks showed induction of AS by AVWI for both $Ldlr^{-/-}/Sort1^{+/+}$ and $Ldlr^{-/-}/Sort1^{-/-}$ (*Figure 1C*), with a reduction in AV opening diameter (sham $Ldlr^{-/-}/Sort1^{+/+}$: 903 ± 25 μm, AVWI $Ldlr^{-/-}/Sort1^{+/+}$: 596 ± 59 μm, $P < 0.001$) (*Figure 1D*) and an increase in AV flow velocity (mm/s) (sham $Ldlr^{-/-}/Sort1^{+/+}$: 1399 ± 79 mm/s, AVWI $Ldlr^{-/-}/Sort1^{+/+}$: 2903 ± 361 mm/s, $P < 0.001$) (*Figure 1E*). The average AV leaflet area (μm^2) across all three AV leaflets was significantly higher in $Ldlr^{-/-}/Sort1^{+/+}$ mice than in $Ldlr^{-/-}/Sort1^{-/-}$ mice following AVWI ($Ldlr^{-/-}/Sort1^{+/+}$: 4355 ± 484 μm, $Ldlr^{-/-}/Sort1^{-/-}$: 2613 ± 296 μm, $P < 0.01$) (see Supplementary material online, *Figure S2E*). Following AVWI, $Ldlr^{-/-}/Sort1^{-/-}$ mice showed reduced fibrosis marked by lower leaflet collagen content ($P < 0.05$) with observable differences of immunoreactive alpha-smooth muscle actin (α-SMA) (*Figure 1F*, right panel). AV opening diameter was measured by echocardiography,

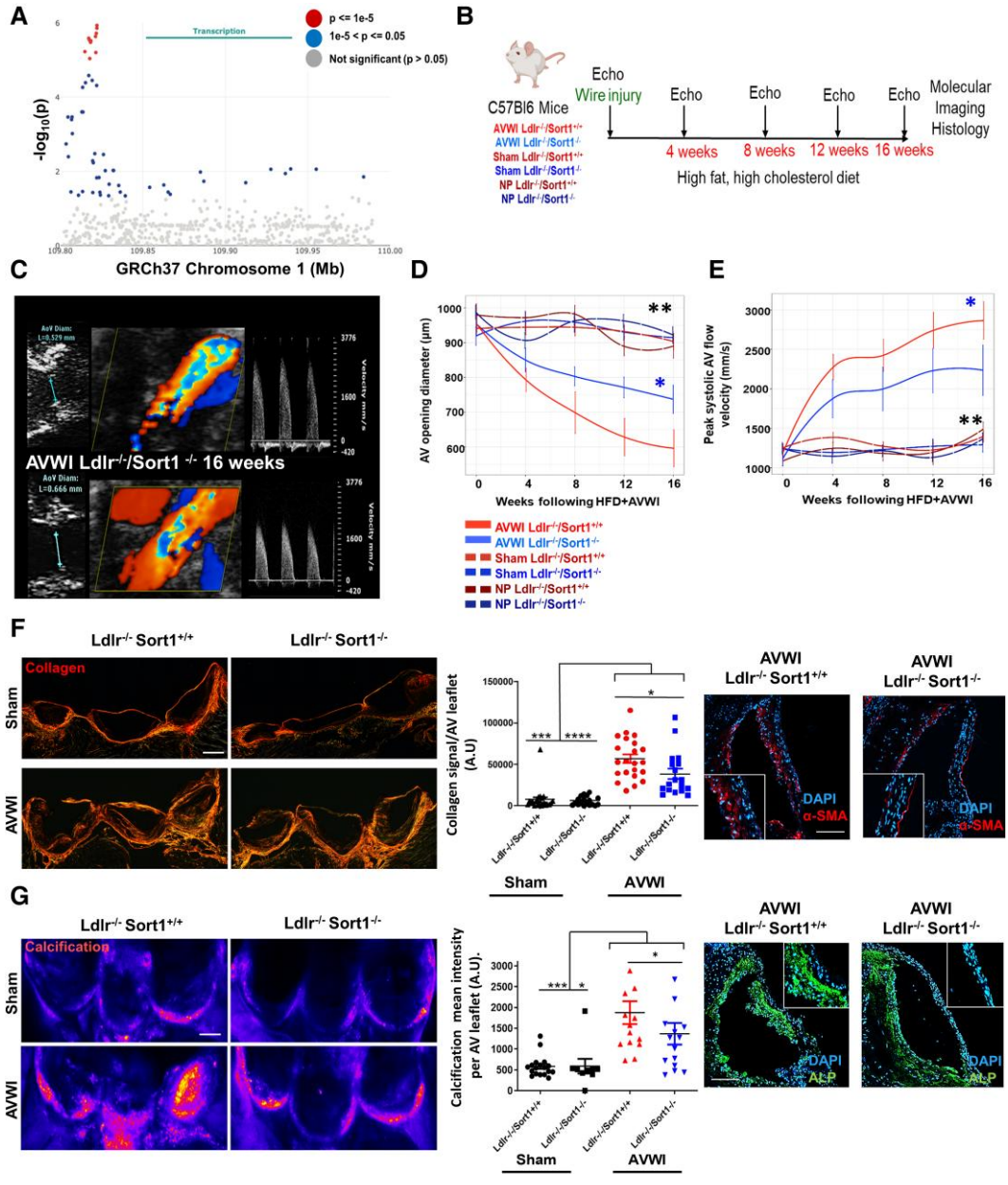

Figure 1 Sortilin-mediated effects on functional and morphometric properties of murine aortic valves. (*A*) Associations with aortic stenosis of 555 variants within 50 kb of *SORT1* in the meta-analysis of the GERA and UK Biobank cohorts (302,597 participants; 6912 cases). GERA, Genetic Epidemiology Research on Adult Health and Aging. (*B*) *In vivo* study design: high-fat, high-cholesterol diet initiation and aortic valve wire injury (AVWI), sham procedure or no procedure at 10 weeks of age, monthly serial echocardiographic exams. (*C*) Left panel: representative parasternal long axis views for aortic valve opening diameter; middle panel: colour flow Doppler of the aortic valve; right panel, flow velocity interrogation of the aortic valve ($n = 10–12$). (*D*) Aortic valve opening diameter and (*E*) peak systolic aortic valve flow velocity for the study groups over 16 weeks, blue asterisk represents AVWI *Ldlr*$^{-/-}$/*Sort1*$^{+/+}$ and black asterisks represent control groups. Aortic valve stenosis and increases in peak systolic aortic valve flow for AVWI *Ldlr*$^{-/-}$/*Sort1*$^{+/+}$ vs. AVWI *Ldlr*$^{-/-}$/*Sort1*$^{-/-}$ (blue asterisk, $P < 0.05$) and for *Ldlr*$^{-/-}$/*Sort1*$^{+/+}$ and *Ldlr*$^{-/-}$/*Sort1*$^{-/-}$ vs. all other groups (black asterisk, $P < 0.01$) over the time of echocardiographic measurements. (*F*) Representative collagen staining of aortic valve leaflets using picrosirius staining. Higher collagen signal and fibrosis detected inAVWI *Ldlr*$^{-/-}$/*Sort1*$^{+/+}$ vs. AVWI *Ldlr*$^{-/-}$/*Sort1*$^{-/-}$ ($P < 0.05$) and greater collagen signal detected in AVWI vs. sham mice *Ldlr*$^{-/-}$/*Sort1*$^{+/+}$ and *Ldlr*$^{-/-}$/*Sort1*$^{-/-}$ ($P < 0.001$ and $P < 0.0001$, respectively). Representative immunofluorescence imaging of myofibroblast activation (α-smooth muscle actin) in aortic valve leaflets. (*G*) Calcification molecular imaging of all three aortic valve leaflets by multiphoton and confocal microscopy. Calcification intensity per aortic valve: increased calcification detected in AVWI *Ldlr*$^{-/-}$/*Sort1*$^{+/+}$ vs. AVWI *Ldlr*$^{-/-}$/*Sort1*$^{-/-}$ ($P < 0.05$) and aortic valve wire injury mice vs. sham *Ldlr*$^{-/-}$/*Sort1*$^{+/+}$ and *Ldlr*$^{-/-}$/*Sort1*$^{-/-}$ ($P < 0.001$ and $P < 0.05$, respectively). Representative immunofluorescence imaging of alkaline phosphatase in aortic valve leaflets. One-way ANOVA performed for statistical analysis (*$P < 0.05$, **$P < 0.01$, ***$P < 0.001$, and ****$P < 0.0001$). Scale bars for (*F* and *G*) (picrosirius and calcification staining): 500 µm. Scale bars for (*F* and *G*) (α-smooth muscle actin and alkaline phosphatase staining):100 µm.

Table 2 Associations of select *SORT1* locus variants with aortic stenosis, with and without adjustment for low-density lipoprotein cholesterol and cholesterol-lowering medication use

Variant	Correlation with lead variant rs599839 (r^2)	CADD C-Score	EA	EAF	GERA and UK Biobank		UK Biobank	
					Odds ratio per EA (95% CI)	*P*	Adjusted odds ratio per EA (95% CI)	Adjusted *P*
rs599839	1.0	0.03	A	0.77	1.11 (1.07–1.16)	1.2×10^{-6}	1.08 (1.02–1.15)	9.1×10^{-3}
rs1277930	1.0	1.08	A	0.77	1.11 (1.07–1.16)	1.4×10^{-6}	1.08 (1.02–1.15)	0.011
rs4970836	0.98	2.58	A	0.77	1.11 (1.06–1.16)	1.9×10^{-6}	1.09 (1.02–1.15)	8.2×10^{-3}
rs583104	0.99	5.79	T	0.77	1.11 (1.06–1.16)	2.3×10^{-6}	1.08 (1.02–1.15)	0.012
rs7528419	0.94	0.88	A	0.78	1.11 (1.06–1.16)	2.6×10^{-6}	1.08 (1.01–1.15)	0.015
rs12740374	0.94	4.10	G	0.78	1.11 (1.06–1.16)	2.9×10^{-6}	1.08 (1.01–1.15)	0.017
rs646776	0.94	1.31	T	0.78	1.11 (1.06–1.16)	3.1×10^{-6}	1.08 (1.02–1.15)	0.014
rs629301	0.93	11.23	T	0.78	1.11 (1.06–1.16)	3.4×10^{-6}	1.08 (1.01–1.15)	0.015
rs4970834	0.63	11.04	C	0.81	1.12 (1.06–1.17)	6.0×10^{-6}	1.08 (1.02–1.16)	0.016
rs602633	0.92	8.83	G	0.78	1.11 (1.06–1.16)	6.3×10^{-6}	1.08 (1.02–1.15)	0.014
rs660240	0.87	15.32	C	0.79	1.11 (1.06–1.16)	9.2×10^{-6}	1.08 (1.01–1.14)	0.020

CADD, combined annotation dependent depletion; EA, effect allele; EAF, effect allele frequency.

which was negatively correlated with AV flow velocity ($P = 0.001$) (see Supplementary material online, *Figure S2F*). Flow velocity was positively correlated with leaflet area ($P < 0.01$) (see Supplementary material online, *Figure S2G*). Additional echocardiographic parameters can be found in the Supplementary material online, *Figure S3A–H*. Left ventricular ejection fraction was significantly lower, left ventricular end-systolic diameters and end-diastolic interventricular septum thickness (IVSed) were higher in AVWI $Ldlr^{-/-}/Sort1^{+/+}$ compared with the respective parameters at baseline and in sham after 16 weeks. AVWI resulted in left ventricular enlargement irrespective of the genetic background.

Valvular calcification was measured by multiphoton-mapped near-infrared fluorescence imaging (see Supplementary material online, *Figure S2H*). AV calcification was significantly lower in $Ldlr^{-/-}/Sort1^{-/-}$ and sham controls than in $Ldlr^{-/-}/Sort1^{+/+}$ following AVWI [$P < 0.001$; mean intensity: AVWI: $Ldlr^{-/-}/Sort1^{+/+}$: 2016 ± 168 (AU), $Ldlr^{-/-}/Sort1^{-/-}$: 1420 ± 153 (AU), $P < 0.05$] (*Figure 1G*). Histological analysis of aortic leaflets showed observable signal differences in ALP staining in $Ldlr^{-/-}/Sort1^{-/-}$ mice compared with $Ldlr^{-/-}/Sort1^{+/+}$ mice (*Figure 1G*, right panel). These results suggest a role for sortilin in mediating fibrosis and calcification in a mouse model of CAVD that can be further investigated in human VICs isolated from CAVD tissue.

Sortilin is identified in calcific aortic valve disease tissue within regions of fibrosis and calcification

Aortic valves obtained from patients with CAVD were processed for tissue-level analysis and VIC isolation (*Figure 2A*; Supplementary material online, *Figure S4A*). Collagen deposits and calcification nodules adjacent to sortilin-expressing cells were observed in fibrosa layers of AVs (*Figure 2B*). Quadruple fluorescence (IF) staining for sortilin, smooth muscle 22-alpha (SM22α), ALP activity and calcification (OsteoSense), identified myofibroblast activation and calcification (*Figure 2C*). While staining of healthy valves from autopsy donors showed negligible SM22α, ALP activity and absence of calcification in relation to CAVD AV (see Supplementary material online, *Figure S4B and C*). Valvular interstitial cells from human AV leaflets were expanded in normal GM and processed for scRNA-seq. Uniform manifold approximation and projections (UMAP) identified heterogeneity in sortilin expression and detected 12 unique VIC population clusters at baseline (*Figure 2D*). Next, VICs were cultured in CM and OM with sortilin siRNA for up to 21 days. We investigated the localization of sortilin in VICs, and identified increased expression of sortilin within the *trans Golgi* apparatus and α-SMA, which were attenuated following sortilin silencing by siSORT1 at day 14 (*Figure 2E*). Sortilin mRNA and protein expression were increased in VICs cultured in OM when compared with CM ($P < 0.05$) over 21 days of culture, which decreased following siSORT1 at days 7, 14, and 21 of culture ($P < 0.0001$) (*Figure 2F and G*, Supplementary material online, *Figure S5*). Overall, sortilin was identified in fibrotic and calcified regions of diseased valves and scRNA-seq identified VIC heterogeneity in sortilin expression.

A subset of human valvular interstitial cells adopts a myofibroblastic-osteogenic phenotype

To further characterize VIC heterogeneity, VICs were cultured in CM and OM for 14 and 21 days and processed for flow cytometry to study their cellular differentiation properties. Three main VIC populations with varying sizes and granularity were identified at day 21 of culture (*Figure 3A*). Overlaid histograms for different media [OM (orange), CM (blue) and compensation control (red)] showed increased expression of vimentin, sortilin, α-SMA, osteopontin, osteocalcin and ALP in VICs (*Figure 3B*). A greater number of double positive VICs for sortilin and myofibroblast and osteogenic-associated markers were identified in OM vs. CM (see Supplementary material online, *Figure S6A*). Single t-SNE plots highlighted clusters with higher sortilin expression in conjunction with the expression of α-SMA, vimentin, osteopontin and

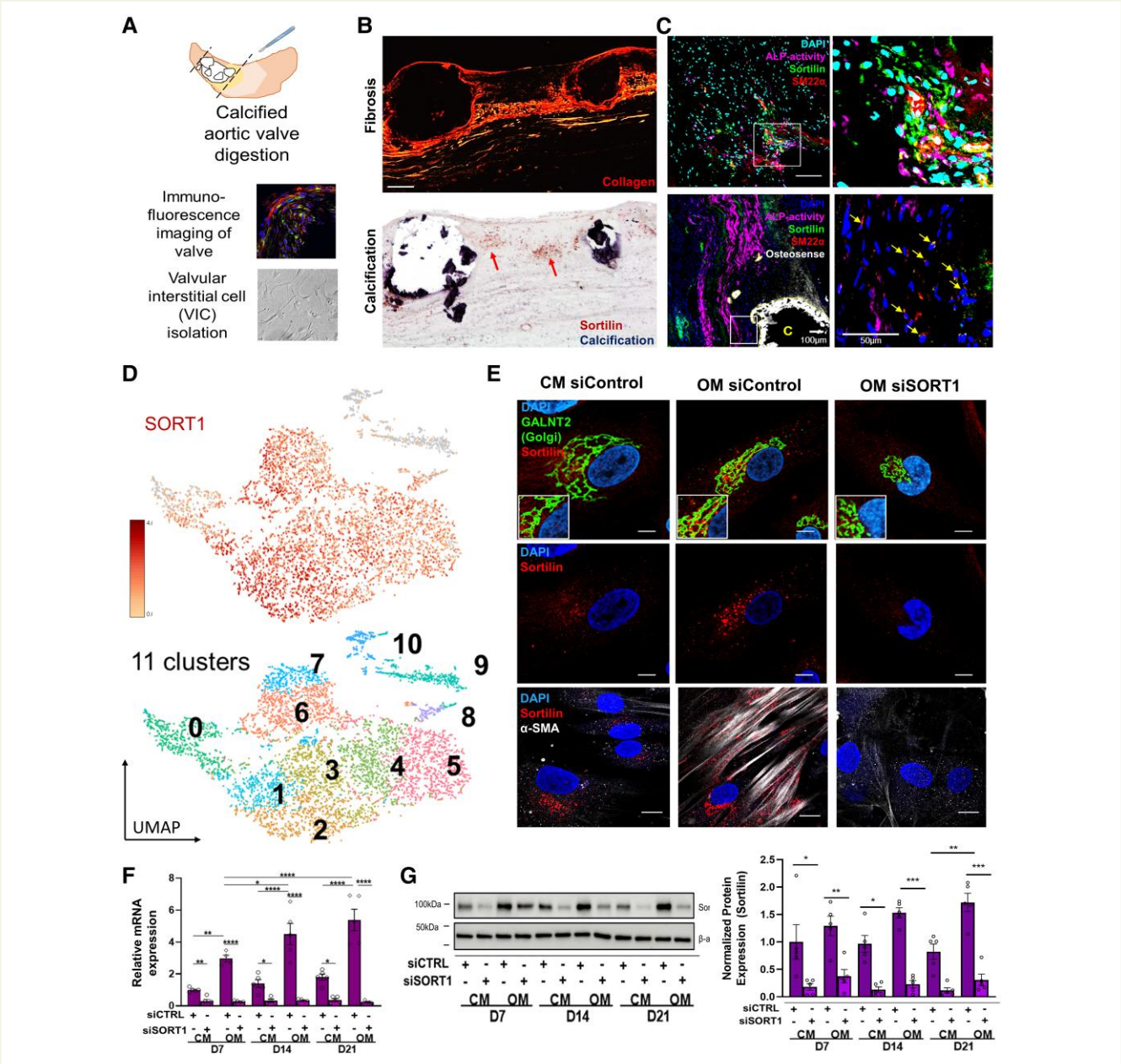

Figure 2 Sortilin is expressed by valvular interstitial cells identified in calcific aortic valve disease. (*A*) Schematic highlighting the use of freshly obtained aortic valve samples from patients with calcific aortic valve disease. Valvular interstitial cells were expanded in growth medium and then stimulated in control or osteogenic media (control media, osteogenic media, respectively). (*B*) Representative imaging of fibrotic (picrosirius) and calcified regions of the aortic valve. Sortilin expressed in fibrotic collagen-rich (top) and calcified aortic valve regions (bottom) ($n = 3$). (*C*) Representative immunofluorescence imaging identifying cells in calcific aortic valve disease samples that co-express sortilin, alkaline phosphatase activity, SM22α, near areas of calcification ($n = 3$). (*D*) Single-cell RNA-sequencing analysis and uniform manifold approximation and projection of valvular interstitial cells expanded in growth media. Uniform manifold approximation and projection highlights overall valvular interstitial cell heterogeneity and heterogeneity in the expression of sortilin ($n = 3$). (*E*) Representative immunofluorescence imaging of valvular interstitial cells cultured in osteogenic media with small interfering RNA sicontrol and siSORT1 for 14 days. Valvular interstitial cells increase the expression of sortilin in osteogenic media conditions. In the bottom panel, valvular interstitial cells co-express sortilin and α-smooth muscle actin ($n = 3$). (*F*) Quantitative polymerase chain reaction ($n = 6$) and (*G*) western blot analysis to identify protein and mRNA transcripts levels of sortilin by valvular interstitial cells over 21 days of culture in osteogenic media sicontrol and siSORT1 conditions ($n = 5$). A significant increase in sortilin detected at day 21 in osteogenic media conditions compared with control media ($P < 0.05$). Two-way ANOVA performed for statistical analysis (*$P < 0.05$, **$P < 0.01$, ***$P < 0.001$, and ****$P < 0.0001$). Scale bars for (*B*) (collagen/calcification staining) 500 μm; (*C*) high magnification 100 μm, low magnification 50 μm. (*E*) 2 μm.

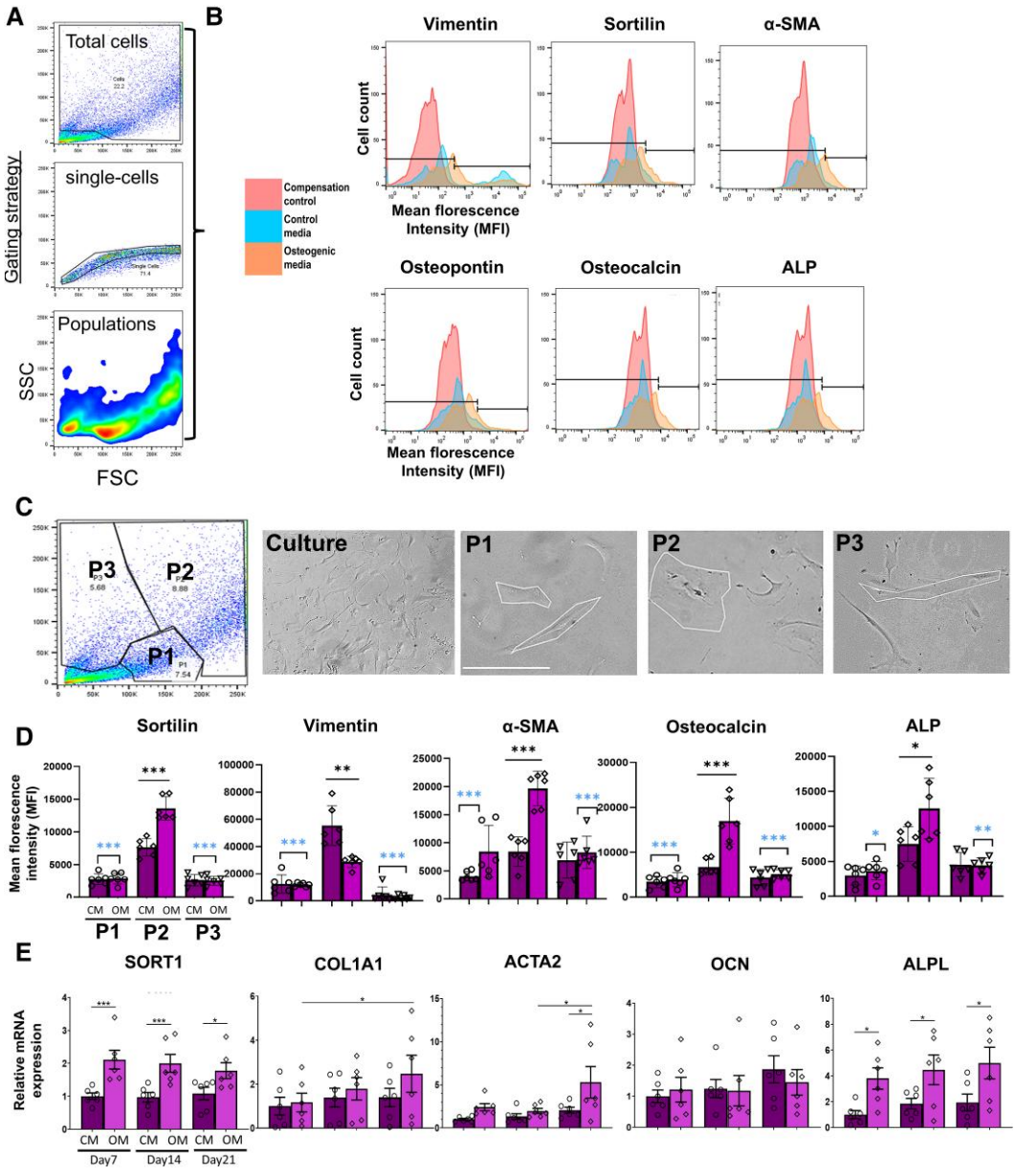

Figure 3 Flow cytometry identifies a subset of valvular interstitial cells that are larger in size and co-express sortilin with myofibroblastic-osteogenic markers. (*A*) Flow cytometry gating strategy to identify mean fluorescence intensities of proteins expressed by valvular interstitial cells cultured in control media and osteogenic media conditions for 21 days. (*B*) Overlapping histograms of mean fluorescence intensities for compensation control, control media and osteogenic media groups. Gates are determined based on compensation controls. Greater mean fluorescence intensities identified by valvular interstitial cells cultured in osteogenic media conditions for myofibroblast activation marker (α-smooth muscle actin) and osteogenic markers (osteopontin, osteocalcin, and alkaline phosphatase) ($n = 5$). (*C*) Gating strategy for three valvular interstitial cell sub-populations based on valvular interstitial cell complexity (side scatter (SSC)) and size (forward scatter (FSC)), where larger-sized valvular interstitial cells are identified in P2 gate, supported by representative bright field images ($n = 6$). (*D*) Quantification of mean fluorescence intensities for myofibroblast and osteogenic proteins expressed by valvular interstitial cells in P1, P2, and P3 gates. Sub-gate P2 includes valvular interstitial cells that increase the expression of sortilin ($P < 0.001$), α-smooth muscle actin ($P < 0.001$), osteocalcin ($P < 0.001$) and alkaline phosphatase ($P < 0.05$) in osteogenic media conditions compared with control media ($n = 6$). Black asterisks identify differences within the P2 gate, whereas blue asterisks represent significant differences between P2 and other respective P-gates with blue asterisks. (*E*) Quantification of myofibroblast and osteogenic mRNA transcript levels by quantitative polymerase chain reaction at days 7, 14, and 21 of osteogenic media culture ($n = 6$). Valvular interstitial cells increase the expression of sortilin in conjunction with increases in COL1A1, ACTA2, and ALPL over 21 days of culture. Two-way ANOVA performed for statistical analysis (*$P < 0.05$, **$P < 0.01$, ***$P < 0.001$, and ****$P < 0.0001$). Scale bar for (*C*), 25 μm.

osteocalcin (see Supplementary material online, *Figure S6B*). The flowSOM algorithm identified 19 VIC sub-populations with varying expression of sortilin, vimentin, α-SMA, osteopontin and osteocalcin (see Supplementary material online, *Figure S7*). VICs cultured in OM constituted at least six sub-populations compared with three in CM, with equal representation of myofibroblastic-osteogenic-associated phenotypes of VICs (see Supplementary material online, *Figure S7*).

Total VICs processed for flow cytometry at day 21 were sorted into three main gates based on density plots (*Figure 3C*). Valvular interstitial cells belonging to the P2 gate displayed osteoblast-like morphologies compared with spindle-shaped VICs identified in P1 and P3 gates (*Figure 3C*). Valvular interstitial cells in the P2 gate significantly increased sortilin expression in OM vs. CM ($P < 0.001$), and to P1 and P3 gates ($P < 0.001$) (*Figure 3D*). VICs in the P2 gate decreased the expression of vimentin in OM vs. CM ($P < 0.01$), but increased the expression of α-SMA, osteocalcin and ALP ($P < 0.05$) (*Figure 3D*). Decreases in vimentin expression in the P2-gate suggests a decline in a fibroblast-phenotype in conjunction with increases in osteogenic phenotypes from day 14 to 21 in osteogenic culture (see Supplementary material online, *Figure S8A and B*). Valvular interstitial cells cultured in OM increased the mRNA-level expression of COL1A1, ACTA2, and ALPL in OM ($P < 0.05$) vs. CM (*Figure 3E*). Collectively, these results suggest that in an osteogenic environment, VICs increase sortilin expression, where a subset of VICs differentiate into a myofibroblastic-osteogenic phenotype, signified by increased expression of COL1A1, α-SMA, osteocalcin, and ALP.

Sortilin-mediated myofibroblast valvular interstitial cell activation is in part regulated by MAPK and YAP signalling and also associated with alkaline phosphatase expression in osteogenic phenotypes

To further investigate the role of sortilin in myofibroblast activation and calcification, VICs were silenced for sortilin by siSORT1 concurrently when cultured in CM and OM for 21 days. Immunofluorescence imaging identified increased expression of α-SMA and COL1A1 by VICs cultured in OM at day 14, which was attenuated with siSORT1 (*Figure 4A*). Specifically, both total collagen and COL1A1 increased in OM, which decreased following siSORT1 (see Supplementary material online, *Figure S9A and B*). The expression of p38 MAPK and YAP/TAZ were explored based on previous identification of MAPK-signalling enrichment and YAP-dependent stiffening in human CAVD tissue.[23,24] Increases in myofibroblast-associated transcripts (COL1A1, ACTA2, TAGLN, and MAPK11) were significantly reduced following siSORT1 ($P < 0.001$) (*Figure 4B*). Trends in decreases of total p38 MAPK protein levels and significant decreases in YAP protein levels ($P < 0.05$) suggest the role of sortilin in VIC myofibroblast activation partly through both the MAPK and YAP pathway (*Figure 4B*; Supplementary material online, *Figure S10*). The addition of a p38 MAPK inhibitor (SB203580) to VIC cultures significantly reduced the expression of myofibroblast-activated genes including ACTA2, calponin (CNN1), myosin heavy chain 11 (MYH11), while also reducing secreted COL1A1 ($P < 0.05$) (see Supplementary material online, *Figure S11A and B*). These results suggest that sortilin partly associates with the MAPK and YAP signalling pathway, which may act as a modulator of VIC differentiation into a myofibroblastic-osteogenic phenotype.

To investigate the osteogenic properties of VICs, ALP expression, ALP activity, and *in vitro* calcium mineral deposition were assessed by qPCR, immunofluorescence imaging, ELISA and Alizarin red staining, respectively. VICs increased the expression of ALP in OM culture vs. CM ($P < 0.0001$), which was significantly reduced following siSORT1 ($P < 0.0001$) (*Figure 4B*). Immunofluorescence imaging of VICs confirmed co-expression of ALP and sortilin signals, which decreased following siSORT1 (*Figure 4C*). VICs increased ALP activity in OM vs. CM ($P < 0.0001$), which decreased following siSORT1 ($P < 0.05$) (*Figure 4D*). Alizarin red staining identified a significant increase in sortilin-mediated deposition of calcium mineral in OM vs. CM ($P < 0.01$), which decreased following siSORT1 ($P < 0.05$) (*Figure 4E*). Silencing sortilin also decreased the expression of associated osteogenic genes including CNN1, MYH11 and OPG (see Supplementary material online, *Figure S12*).

Label-free proteomic profiling of valvular interstitial cells following the silencing of sortilin

Global proteomics was implemented to identify sortilin-mediated changes in protein profiles and signalling pathways following VIC culture in osteogenic conditions, with and without silencing sortilin. Principal component analysis and a heatmap of non-filtered data (2611 proteins with ≥2 peptides) display sample clustering and contrast between the changing proteome following siSORT1 (see Supplementary material online, *Figure S13A and B*). A total of 580 differentially abundant proteins were identified using two group comparisons of VICs cultured in CM and OM (Supplementary material online, *Figure S14*). Cluster 1 comprised proteins that were predominantly enriched in OM, whereas Cluster 2 comprised proteins that were decreased in OM. Pathway networks based on top differentially abundant proteins between CM and OM conditions confirmed molecular pathways associated with myofibroblastogenesis, ECM remodelling, collagen, and ossification (see Supplementary material online, *Figure S15*). Next, we investigated proteins enriched under sicontrol conditions relative to siSORT1 (*Figure 4G*). Pathway enrichment analysis of 947 enriched proteins in si-control vs. siSORT1 suggested decreased expression of proteins associated with myofibroblastogenesis, ECM organization, collagen-related pathways and cell differentiation (see Supplementary material online, *Figure S16*). Collectively, both transcript and protein-level analyses suggest a role of sortilin in myofibroblastogenesis in addition to inducing ALP activity and *in vitro* calcification.

Single-cell transcriptomics identifies five novel sub-populations of valvular interstitial cells exclusively in osteogenic conditions

VICs cultured in GM (Day 0), CM and OM for 14 and 21 days, were sorted and processed using the 10× genomics pipeline. Four donors were sequenced per condition (GM, CM, OM) and day of culture (days 0, 14, and 21), integrated using Harmony (v1) in R,[25] and projected using UMAP. Individual donor–donor variability (see Supplementary material online, *Figure S17A*). UMAP projections showed overlap between VICs cultured in both GM and CM (pink and purple, respectively), VICs unique to OM (maroon), and a common group of cells (highlighted by red square) (*Figure 5A*). Separation of UMAP projections based on days of culture, identified new clusters on day 14 (green), with an exclusive new population of cells in OM at day 21 [red square (grey)] (*Figure 5B*). The Louvain algorithm with resolution parameter 0.5, found 12 independent clusters of cells across the three media and days of culture (*Figure 5C*). Violin plots display the expression of SORT1 in 10 out

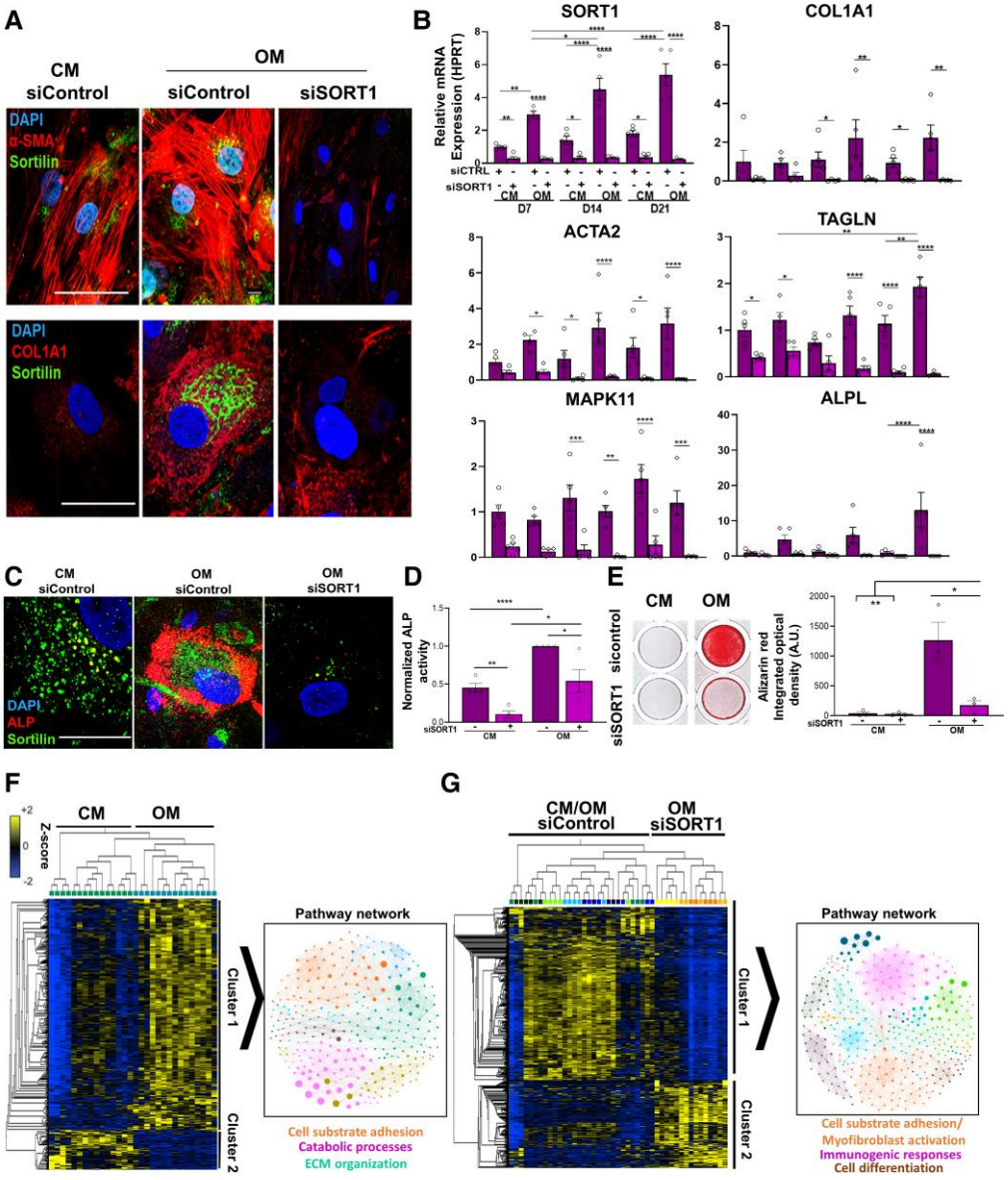

Figure 4 Silencing sortilin decreases valvular interstitial cell myofibroblastic-osteogenic phenotypes and decreases *in vitro* calcification. (*A*) Representative immunofluorescence imaging of valvular interstitial cells cultured in osteogenic media conditions with small interfering RNA SORT1 silencing. Valvular interstitial cells with decreased expression of sortilin also decreased the expression of myofibroblast activation proteins α-smooth muscle actin, collagen 1A1 compared with control media (CM)sicontrol and osteogenic media (OM) sicontrol groups ($n = 3$). (*B*) Quantification of myofibroblast and osteogenic mRNA transcript levels by quantitative polymerase chain reaction at days 7, 14, and 21 of culture. Plus indicates siSORT1 and minus indicates sicontrol. Valvular interstitial cells decrease the expression of myofibroblastic-osteogenic transcripts when sortilin is silenced in osteogenic media conditions over 21 days of culture ($P < 0.001$) ($n = 5$). (*C*) Representative immunofluorescence imaging identifying sortilin and alkaline phosphatase by valvular interstitial cells cultured in osteogenic conditions ($n = 3$). (*D*) Quantification of alkaline phosphatase activity shows decreased activity following siSORT1 ($P < 0.05$) ($n = 4$, Day 14). (*E*) Alizarin staining to identity *in vitro* calcification. SORT1 silencing significantly reduces valvular interstitial cell calcification ($P < 0.05$) ($n = 3$). (*F*) Label-free proteomics by two group comparisons via *t*-test, false discovery rate $q < 0.05$. Heat map representing statistically filtered protein abundances for each valvular interstitial cell sample further underscore the contrast between the culture conditions, control media and osteogenic media, including 580 differentiating protein variables ($n = 5$). Right panel: schematic pathway network depicting Gene Ontology Biological Process terms enriched in differentially expressed proteins (see Supplementary figures for labeled pathways and figure details). (*G*) Heat map representing statistically filtered protein abundances for valvular interstitial cell sample cultured in control media and osteogenic media and treated with sicontrol or with siSORT1 treatment (including timepoints days 7, 14, and 21, two group comparison between by *t*-test sicontrol vs. siSORT1, $q < 0.05$). Heat map underscores the contrast in valvular interstitial cell protein profiles after sortilin silencing, including 947 differentiating protein variables ($n = 5$). Proteins decreased in valvular interstitial cells are represented in blue and increased proteins are represented in yellow. Right panel: schematic pathway network depicting Gene Ontology Biological Process terms enriched in Cluster 1 (i.e. enriched in sicontrol; see Supplementary figures for labeled pathways and figure details). Two-way ANOVA performed for statistical analysis (*$P < 0.05$, **$P < 0.01$, ***$P < 0.001$, and ****$P < 0.0001$). Scale bar for (*A* and *C*): 25 μm.

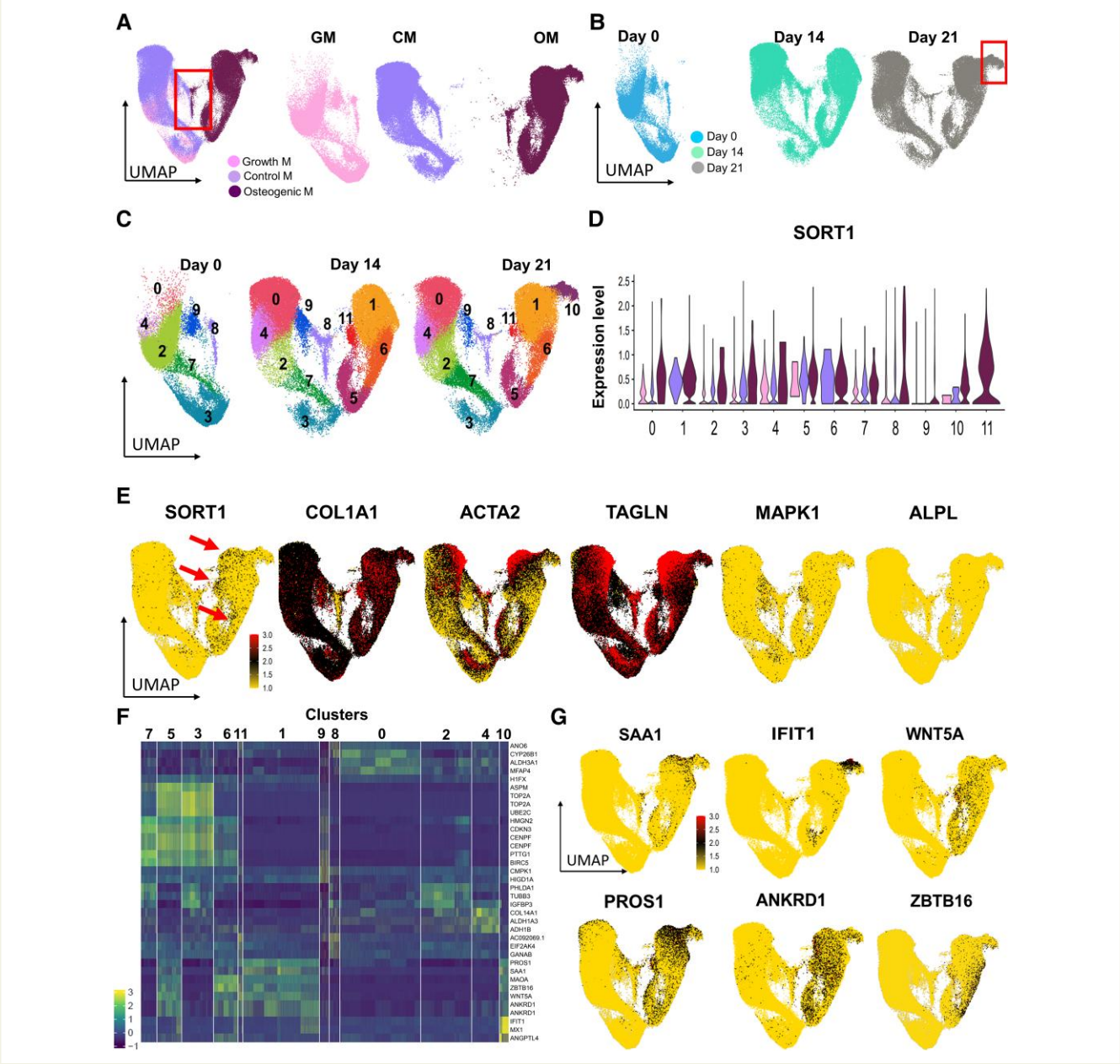

Figure 5 Single-cell RNA-sequencing identifies heterogeneity in valvular interstitial cell cultures and novel clusters in osteogenic conditions. (*A*) Uniform manifold approximation and projection projections of valvular interstitial cells sequenced at days 0, 14, and 21 in growth media (GM), control media (CM) and osteogenic media (OM). Common cluster to all conditions highlighted by the box. Deconstructed uniform manifold approximation and projection based on culture conditions. (*B*) Deconstructed uniform manifold approximation and projection highlighting emergence of valvular interstitial cell clusters based on the day of culture (Day 0, Day 14 , and Day 21). Novel valvular interstitial cell population at Day 21 in osteogenic media highlighted by box. (*C*) Uniform manifold approximation and projection projections highlighting heterogeneity in valvular interstitial cell cultures by identifying 12 unique clusters over 21 days of culture, in addition to the emergence novel Cluster 10 at day 21 of culture only in osteogenic media conditions. (*D*) Violin plots identifying the expression of SORT1 in 12 valvular interstitial cell clusters based on culture conditions (growth media, control media, and osteogenic media). SORT1 increases in osteogenic media conditions in all clusters, whereas SORT1 is exclusively identified in osteogenic media conditions for Cluster 11. (*E*) Uniform manifold approximation and projection projections of SORT1 and myofibroblast activation genes (COL1A1, ACTA2, TAGLN, and MAPK11) and osteogenic gene (alkaline phosphatase) in valvular interstitial cell populations. Enrichment of SORT1 identified in clusters (arrows) detected only in osteogenic media conditions; based on intensity scale. (*F*) Heat map highlighting the enrichment of top 50 genes per cluster. (*G*) Uniform manifold approximation and projection projections of top enriched genes identified mainly in osteogenic media conditions. $n = 3$ for each culture condition and time point. Uniform manifold approximation and projection and heat map display normalized gene expression.

of 12 clusters in OM conditions (maroon) (*Figure 5D*). The composition of each cluster based on culture media and day of culture found in Supplementary material online, *Figure S17B* and *C*.

We then assessed the distribution of normalized expression patterns using UMAP for several genes of interest, where SORT1 was primarily enriched in OM-predominant regions (red arrows) with enriched expression of COL1A1, ACTA2, TAGLN, and MAPK1, supporting our *in vitro* results of an activated myofibroblastic phenotype (*Figure 5E*). Splitting of UMAP projections based on the day of culture, showed lower expression of SORT1, ACTA2, TAGLN, MAPK1, and ALPL in GM (day 0), which increased in OM by day 21 (see Supplementary material online, *Figure S18*). These findings suggest that osteogenic conditions propagate myofibroblastic-osteogenic phenotypes in VICs and that sortilin is expressed in VICs with greater pathogenic potential.

Expression patterns of various myofibroblastic-osteogenic-associated genes across 12 clusters are shown in Supplementary material online, *Figure S19* revealing consistent patterns of cell heterogeneity. We further classified clusters based on culture conditions (GM, CM, or OM) (see Supplementary material online, *Figure S20A and B*). To identify the top differentially expressed genes per cluster, we show a heatmap illustrating top 25 differentially expressed genes per cluster (*Figure 5F*; Supplementary material online, *Figure S21*), where top enriched genes in OM clusters included serum amyloid A1 (SAA1), interferon induced protein with tetratricopeptide repeats (IFIT1), WNT5A, protein S, ankyrin repeat domain 1 and zinc finger and BTB Domain Containing 16 (*Figure 5G*; Supplementary material online, *Figure S20B*). The analysis identified the emergence of a new population of VICs that arises in the late stage (day 21) of osteogenic culture, which may be a disease-driving population in CAVD.

Single-cell transcriptomics of valvular interstitial cells identifies a novel inflammatory myofibroblastic-osteogenic valvular interstitial cell population

We performed pseudotime trajectory analysis using slingshot,[26] which can infer multiple lineages of VICs arising from baseline conditions, over 21 days of culture (*Figure 6A*; Supplementary material online, *Figure S22A*). In OM conditions, Cluster 10 (day 21: 99% cells, day 14: 0.84% cells, and day 0: 0.14% cells) and Cluster 11 (day 21: 25.6% cells and day 14: 74.4% cells) were identified as terminal clusters, whereas Cluster 1 (day 21: 55% cells and day 14: 45% cells) bridged Clusters 10 and 11 (*Figure 6A*). The top differentially expressed genes in the main OM clusters (1, 6, 10, and 11) are represented on a heat map (*Figure 6B*), with relevant genes extracted and plotted on violin plots (*Figure 6C*). Cluster 5 was dropped from the analysis due to the high expression of genes associated with cell proliferation (TOP2A), potentially due to its role as a transitionary cluster between CM and OM (see Supplementary material online, *Figures S19* and *S20*). A detailed heatmap identifying top differentially expressed genes based on pseudotime analysis can be found in Supplementary material online, *Figure S22B*. Osteogenic media clusters showed the enrichment of genes implicated in myofibroblastic-osteogenic and inflammatory phenotypes (*Figure 6C*). Violin plots showed increased expression levels of ACTA2, COL1A1, WNT5A, and calmodulin in OM rich clusters, with enrichment of inflammatory markers including IFIT1, MX1, IL6, and SAA1 in Cluster 10 (*Figure 6C*). These results suggest that a subset of VICs with increased expression of sortilin and myofibroblastic-osteogenic phenotypes, undertakes an inflammatory phenotype, which emerges at day 21 in osteogenic culture (Cluster 10). To confirm whether sortilin is the key regulator in the emergence of IMO phenotype (IMO-VIC), VICs ($n = 6$) were processed for scRNA-seq following the silencing of sortilin. Quality control and donor–donor variability can be found in Supplementary material online, *Figure S23A*. UMAP projections identified VIC clusters based on CM and OM culture media (maroon and purple) and sicontrol and siSORT1 conditions (grey and black) (*Figure 6D*). Furthermore, 11 distinct VIC clusters were identified in SORT1 siRNA experiments, whereas slingshot pseudotime analysis identified Clusters 1 and 4 as terminal clusters detected only in siSORT1 conditions (*Figure 6E*). UMAP projections of Clusters 1 and 4 (siSORT1, red box), identified decreased expression of SORT1, ACTA2, COL1A1, WNT5A, IL-6, and SAA1 (*Figure 6F*) and VIM, TAGLN, CNN1, CXCL8, CALD1 compared with sicontrol group (see Supplementary material online, *Figure S23B and C*). To validate these results, VICs co-expressing sortilin, SM22α, IL-6 and WNT5A were identified in CAVD tissue (*Figure 6G*). Silencing sortilin reduced the expression and secretion of IL-6, and transcript expression of IL-6 and WNT5A in VICs (see Supplementary material online, *Figure S24*). These results suggest the presence of VICs with an IMO phenotype in CAVD tissue.

Discussion

This study combined a systems biology strategy with multi-omic approaches to identify the stages of VIC pathologic transformation and to elucidate the role of sortilin in CAVD. Genetic associations in two large-scale, human cohorts support the contribution of the *SORT1* locus to AS independent of low-density lipoprotein cholesterol, consistent with previous work demonstrating an effect on abdominal aortic aneurysm independent of low-density lipoprotein cholesterol.[27] Sortilin, a type I membrane glycoprotein that mediates protein transport was identified and co-expressed in regions of fibrosis and calcification in CAVD tissues. The *in vivo* model of CAVD demonstrated improvements in AS, fibrosis and calcification following wire injury in sortilin and Ldlr-deficient mice. VICs isolated from human CAVD tissues increased the expression of myofibroblast-associated markers (α-SMA, SM22α, MAPK and COL1a1) and osteogenic markers (ALP) when cultured in osteogenic conditions. The attenuation of sortilin expression decreased the presence of myofibroblastic-osteogenic phenotypes. The activation of VICs with myofibroblastic phenotypes was dependent on sortilin and in part regulated by MAPK and YAP. To broaden the scope of this study, we analysed VIC heterogeneity and identified VIC sub-populations with fibrotic and calcific phenotypes. ScRNA-seq identified a subset of VICs, that emerged during the late stage of osteogenic transition, with combined IMO-VICs phenotype, which were identified in human CAVD tissue (*Structured Graphical Abstract*). This study highlights a novel disease-driving VIC population that may be a valuable target to slow the progression of CAVD.

Our group and others have previously documented the role of p38 MAPK in atherosclerosis and AV sclerosis.[23,28,29] Circulating osteogenic and inflammatory factors are known to stimulate p38 MAPK-signalling pathways that in turn activate myofibroblast formation by increasing α-SMA.[30] In our studies, VICs decreased mRNA levels of MAPK11 and a trend towards decreased total p38 MAPK protein following sortilin inhibition was observed, while P-p38 MAPK/p38 MAPK ratio was not changed. Inhibiting the activity of p38 MAPK decreased myofibroblast phenotypes, including ACTA2, TAGLN, and collagen secretion. It is possible that the timepoints chosen in this experiment did not capture significant changes in P-p38 MAPK, as phosphorylation states are transient, and time and culture sensitive. To explore additional mechanisms of fibrosis, the Hippo-YAP/TAZ pathway was characterized. Silencing sortilin at day 21 significantly reduced the expression of YAP protein. Previous studies have identified YAP signalling in both

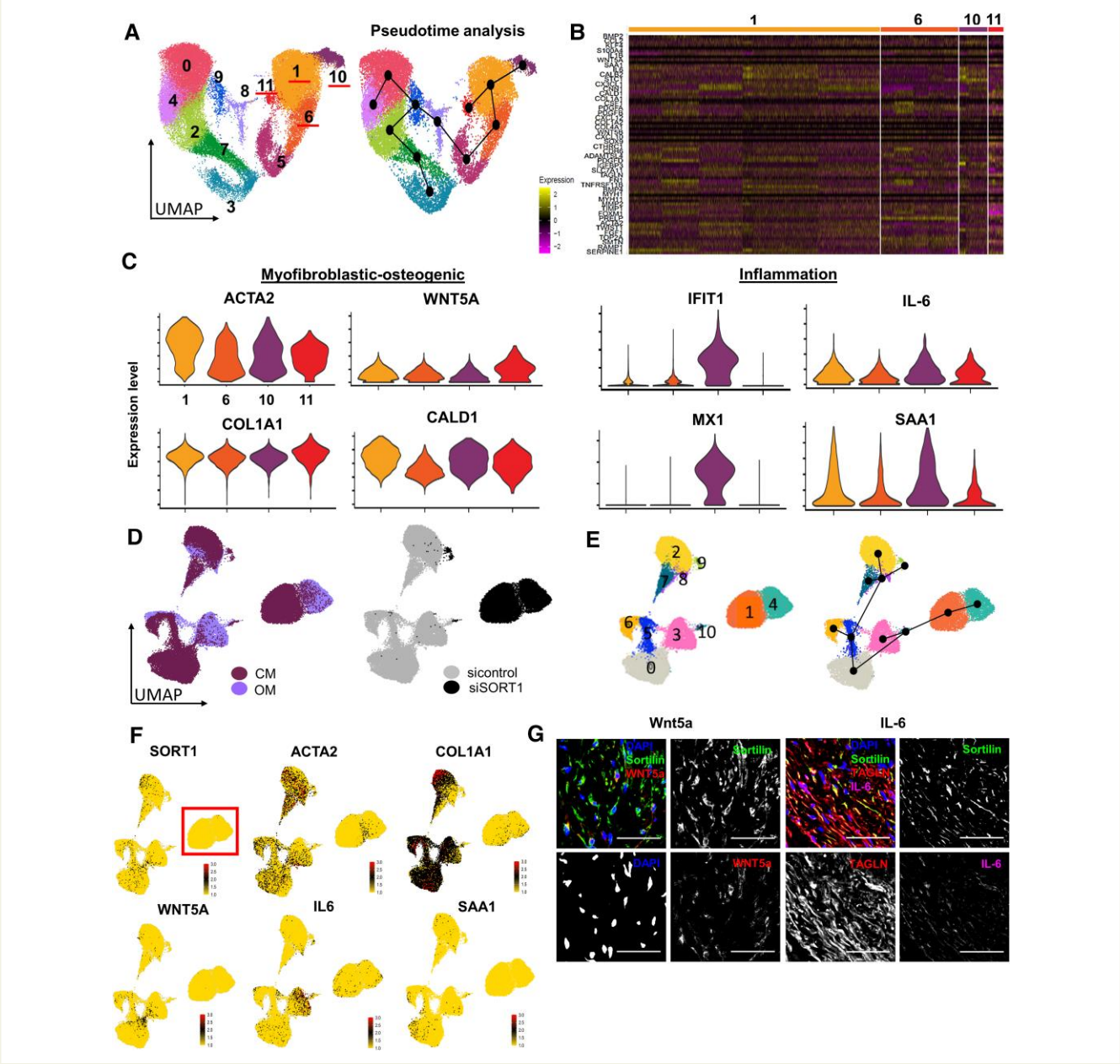

Figure 6 A distinct cluster emerges in osteogenic conditions that represents an inflammatory myofibroblastic-osteogenic phenotype-valvular interstitial cell. (*A*) Uniform manifold approximation and projection highlighting (underline) the clusters in osteogenic media conditions that are further analysed. Pseudotime analysis (slingshot) identifies baseline clusters (3 and 4) and terminal clusters (10 and 11). (*B*) Heat map displaying enriched genes in Clusters 1, 6, 10, and 11, identified only in osteogenic media conditions. (*C*) Violin plots identifying the expression levels of genes enriched in Clusters 1, 6, 10, 11. Cluster 10 exhibits both myofibroblastic-osteogenic and inflammatory phenotypes. (*D*) Single-cell RNA-sequencing analysis and uniform manifold approximation and projection projections of valvular interstitial cells transfected with sicontrol and siSORT1 for 21 days in osteogenic media conditions. Clusters are identified based on culture media and small interfering RNA treatment. (*E*) Uniform manifold approximation and projection projections highlighting the 11 clusters identified in transfected sicontrol and siSORT1 valvular interstitial cells. Pseudotime analysis identifies various cell trajectories from Clusters 0, 3, 5, 6 and 10 (sicontrol) to Clusters 1 and 4 (siSORT1). (*F*) Uniform manifold approximation and projection projections highlighting enriched genes from (*B*). Decreases in the expression of SORT1, ACTA2, COL1A1, WNT5A, IL6, and serum amyloid A1 identified in Clusters 1 and 4, following siSORT1 at 21 days of culture. (*G*) Representative immunofluorescence imaging of human aortic valves that identify the co-expression of sortilin, SM22α and IL-6 and sortilin with WNT5a ($n = 3$). Single-cell RNA-sequencing: $n = 3$ for control media sicontrol and CMsiSORT1 groups and $n = 5$ for osteogenic media sicontrol and siSORT1 groups). Uniform manifold approximation and projection and heat map display normalized gene expression. Scale bar for (*G*): 100 μm.

cardiac fibrosis[31] and AV calcification and stiffening.[24,32] It is likely that various pathways including p38 MAPK and Hippo pathway are involved in regulating AV fibrosis, calcification and increased stiffness, under the regulation of sortilin in CAVD.

ALP is a key factor involved in mineralization and osteoblast differentiation in cardiovascular calcification.[33] VICs increased the activity of ALP and calcium deposition in osteogenic conditions, which was reduced following sortilin silencing. In addition to ALP, VICs increased the expression of osteogenic genes including RAB11A, RUNX2, BMP4 that were not decreased following sortilin silencing. It is possible that sortilin does not directly regulate the expression of these osteogenic genes, but instead, induces VIC differentiation into an inflammatory and myofibroblastic phenotype whose ALP activity and calcifying potential increase in pathology.

Proteomics data identified sortilin as the third most enriched protein in VICs when cultured in OM, where pathway analysis identified decreases in proteins associated with cell substrate adhesion, immunogenic responses, and cell differentiation following sortilin silencing. To identify specific subpopulations that actively undertake pathological phenotypes in CAVD, we further performed scRNA-seq. ScRNA-seq is a novel technology that allows the identification of disease-driving populations for targeted therapeutics.[34] A recent study identified heterogeneity in mouse interstitial cells at different stages of valve development.[35] Interstitial cells from mouse pooled aortic and mitral valves displayed properties of matrifibrocytes, with pro-calcifying properties following cardiac injury.[36] Another study identified functional interactions between resident AV subpopulations, detecting three subtypes of interstitial cells.[37] Our group recently characterized a disease-driving population of sorted CD44^{high} VICs with pro-calcifying potential isolated from human CAVD tissue.[38] We chose to advance prior work by not pre-selecting VIC sub-populations but to characterize human VIC heterogeneity and to identify VIC subsets that may drive fibrosis and calcification concurrently.

Exploring heterogeneity of single cells, RNA-seq analysis of VICs identified 12 distinct VIC clusters, where five clusters were predominantly identified in osteogenic conditions with enriched sortilin expression. In concordance with qPCR and western blot data, sortilin was expressed and sustained at both early (day 14) and late stages (day 21) of osteogenic stimulation. Myofibroblast-associated markers, ACTA2, TAGLN, and COL1A1 were expressed by all clusters, but were enriched in OM clusters. This suggests that VIC subsets display a spectrum of fibroblast-myofibroblast activation, but certain VIC subsets exhibit a more profound myofibroblast phenotype. ALPL expression was not significantly increased in OM clusters, but enrichment was identified in OM-predominant clusters. Trajectory analysis identified Cluster 11 with the highest expression of sortilin which transitioned into Cluster 1 with high ACTA2 expression, leading to Cluster 10, which only emerged in osteogenic conditions at day 21. Further analyses identified increased expression of WNT5a and immunological phenotypes including IL-6, IFIT1, and SAA1. Noncanonical WNT signalling pathway was previously identified in CAVD, where WNT5a drove mineral deposition and calcification.[39] These results cumulatively suggest that sortilin is a key mediator in transitioning VICs into an activated myofibroblast phenotype, where a novel VIC subpopulation adapts a combined inflammatory, fibrotic and pro-calcification phenotype. Targeting this phenotype may delay or diminish the chronic presentation of fibrosis and calcification observed in CAVD.

One of the limitations of single-cell analysis is the inability to combine data from siSORT1 experiments with the original data of non-silenced VICs due to differences in the number of features between experiments. Combining these data would demarcate IMO-VICs in siSORT1 experiments; however, nevertheless we demonstrate IMO-VICs in the siRNA data by documenting decreases in IMO-VIC phenotypic associated genes including SORT1, COL1A1, ACTA2, WNT5A IL-6, and SAA1.

Taken together, the multi-omic approaches identified that sortilin drives the transition of a dominant subset of VICs with myofibroblast properties, which differentiate into a distinct subset of IMO-VICs with IMO phenotypes (see Supplementary material online, *Figure S25*). To our knowledge, this is the first scRNA-seq study to document the heterogeneity of 12 VIC clusters in human CAVD and to identify sortilin as a key regulator in the differentiation of activated VICs into a newly described pathological IMO phenotype. Future studies will explore whether WNT5A is an upstream target of sortilin in CAVD. A strategy to target sortilin and prevent the emergence of IMO-VICs may hold promise to tackle the pathophysiological CAVD cascade at multiple levels.

Acknowledgements

The authors thank Dr Carlijn Bouten for providing CNA35-OG488 collagen probe and the single-cell and immunology flow cytometry facility at Brigham and Women's Hospital.

Supplementary data

Supplementary data is available at *European Heart Journal* online.

Conflict of interest: E.A. has participated in advisory board for Elastrin Therapeutics; G.T. has received consulting fees from Ionis Pharmaceuticals and has participated in advisory boards for Amgen and Sanofi.

Funding

This work was supported by National Institutes of Health grants (NIH) R01HL147095, R01HL141917, and R01HL136431 to E.A and K25HL150336 to A.H. G.T. and J.C.E. hold an operating grant from the Canadian Institutes for Health Research, and G.T. holds operating grants from the Heart and Stroke Foundation of Canada and the NIH (R01 HL128550).

References

1. Yadgir S, Johnson CO, Aboyans V, Adebayo OM, Adedoyin RA, Afarideh M, *et al.* Global, regional, and national burden of calcific aortic valve and degenerative mitral valve diseases, 1990–2017. *Circulation* 2020;**141**:1670–1680. https://doi.org/10.1161/CIRCULATIONAHA.119.043391
2. Lerman DA, Prasad S, Alotti N. Calcific aortic valve disease: molecular mechanisms and therapeutic approaches. *Eur Cardiol* 2015;**10**:108–112. https://doi.org/10.15420/ecr.2015.10.2.108
3. Galeone A, Brunetti G, Oranger A, Greco G, Di Benedetto A, Mori G, *et al.* Aortic valvular interstitial cells apoptosis and calcification are mediated by TNF-related apoptosis-inducing ligand. *Int J Cardiol* 2013;**169**:296–304. https://doi.org/10.1016/j.ijcard.2013.09.012
4. Kraler S, Blaser MC, Aikawa E, Camici GG, Luscher TF. Calcific aortic valve disease: from molecular and cellular mechanisms to medical therapy. *Eur Heart J* 2022;**43**:683–697. https://doi.org/10.1093/eurheartj/ehab757
5. Rutkovskiy A, Malashicheva A, Sullivan G, Bogdanova M, Kostareva A, Stenslokken KO, *et al.* Valve interstitial cells: the key to understanding the pathophysiology of heart valve calcification. *J Am Heart Assoc* 2017;**6**:e006339. https://doi.org/10.1161/JAHA.117.006339
6. Chen JH, Yip CY, Sone ED, Simmons CA. Identification and characterization of aortic valve mesenchymal progenitor cells with robust osteogenic calcification potential. *Am J Pathol* 2009;**174**:1109–1119. https://doi.org/10.2353/ajpath.2009.080750
7. Small A, Kiss D, Giri J, Anwaruddin S, Siddiqi H, Guerraty M, *et al.* Biomarkers of calcific aortic valve disease. *Arterioscler Thromb Vasc Biol* 2017;**37**:623–632. https://doi.org/10.1161/ATVBAHA.116.308615
8. Rogers MA, Aikawa E. Unbiased omics identifies mechanistic regulators of calcific aortic valve disease. *Eur Heart J* 2021;**42**:2948–2950. https://doi.org/10.1093/eurheartj/ehab381

9. Pawade TA, Doris MK, Bing R, White AC, Forsyth L, Evans E, *et al.* Effect of denosumab or alendronic acid on the progression of aortic stenosis: a double-blind randomized controlled trial. *Circulation* 2021;**143**:2418–2427. https://doi.org/10.1161/CIRCULATIONAHA.121.053708
10. Mack MJ, Leon MB, Thourani VH, Makkar R, Kodali SK, Russo M, *et al.* Transcatheter aortic-valve replacement with a balloon-expandable valve in low-risk patients. *N Engl J Med* 2019;**380**:1695–1705. https://doi.org/10.1056/NEJMoa1814052
11. O'Donnell CJ, Kavousi M, Smith AV, Kardia SL, Feitosa MF, Hwang SJ, *et al.* Genome-wide association study for coronary artery calcification with follow-up in myocardial infarction. *Circulation* 2011;**124**:2855–2864.
12. Goettsch C, Kjolby M, Aikawa E. Sortilin and its multiple roles in cardiovascular and metabolic diseases. *Arterioscler Thromb Vasc Biol* 2018;**38**:19–25. https://doi.org/10.1161/ATVBAHA.117.310292
13. Kjolby M, Andersen OM, Breiderhoff T, Fjorback AW, Pedersen KM, Madsen P, *et al.* Sort1, encoded by the cardiovascular risk locus 1p13.3, is a regulator of hepatic lipoprotein export. *Cell Metab* 2010;**12**:213–223. https://doi.org/10.1016/j.cmet.2010.08.006
14. Patel KM, Strong A, Tohyama J, Jin X, Morales CR, Billheimer J, *et al.* Macrophage sortilin promotes LDL uptake, foam cell formation, and atherosclerosis. *Circ Res* 2015;**116**:789–796. https://doi.org/10.1161/CIRCRESAHA.116.305811
15. Aikawa E, Aikawa M, Libby P, Figueiredo JL, Rusanescu G, Iwamoto Y, *et al.* Arterial and aortic valve calcification abolished by elastolytic cathepsin S deficiency in chronic renal disease. *Circulation* 2009;**119**:1785–1794. https://doi.org/10.1161/CIRCULATIONAHA.108.827972
16. Kaiser Y, van der Toorn JE, Singh SS, Zheng KH, Kavousi M, Sijbrands EJG, *et al.* Lipoprotein(a) is associated with the onset but not the progression of aortic valve calcification. *Eur Heart J* 2022;**43**:3960–3967. https://doi.org/10.1093/eurheartj/ehac377
17. Goettsch C, Hutcheson JD, Aikawa M, Iwata H, Pham T, Nykjaer A, *et al.* Sortilin mediates vascular calcification via its recruitment into extracellular vesicles. *J Clin Invest* 2016;**126**:1323–1336. https://doi.org/10.1172/JCI80851
18. Yutzey KE, Demer LL, Body SC, Huggins GS, Towler DA, Giachelli CM, *et al.* Calcific aortic valve disease: a consensus summary from the Alliance of Investigators on Calcific Aortic Valve Disease. *Arterioscler Thromb Vasc Biol* 2014;**34**:2387–2393. https://doi.org/10.1161/ATVBAHA.114.302523
19. Gomel MA, Lee R, Grande-Allen KJ. Comparing the role of mechanical forces in vascular and valvular calcification progression. *Front Cardiovasc Med* 2018;**5**:197. https://doi.org/10.3389/fcvm.2018.00197
20. Herwig R, Hardt C, Lienhard M, Kamburov A. Analyzing and interpreting genome data at the network level with ConsensusPathDB. *Nat Protoc* 2016;**11**:1889–1907. https://doi.org/10.1038/nprot.2016.117
21. Hao Y, Hao S, Andersen-Nissen E, Mauck WM III, Zheng S, Butler A, *et al.* Integrated analysis of multimodal single-cell data. *Cell* 2021;**184**:3573–87.e29. https://doi.org/10.1016/j.cell.2021.04.048
22. Stuart T, Butler A, Hoffman P, Hafemeister C, Papalexi E, Mauck WM III, *et al.* Comprehensive integration of single-cell data. *Cell* 2019;**177**:1888–902.e21. https://doi.org/10.1016/j.cell.2019.05.031
23. Schlotter F, Halu A, Goto S, Blaser MC, Body SC, Lee LH, *et al.* Spatiotemporal multi-omics mapping generates a molecular atlas of the aortic valve and reveals networks driving disease. *Circulation* 2018;**138**:377–393. https://doi.org/10.1161/CIRCULATIONAHA.117.032291
24. Santoro R, Scaini D, Severino LU, Amadeo F, Ferrari S, Bernava G, *et al.* Activation of human aortic valve interstitial cells by local stiffness involves YAP-dependent transcriptional signaling. *Biomaterials* 2018;**181**:268–279. https://doi.org/10.1016/j.biomaterials.2018.07.033
25. Korsunsky I, Millard N, Fan J, Slowikowski K, Zhang F, Wei K, *et al.* Fast, sensitive and accurate integration of single-cell data with Harmony. *Nat Methods* 2019;**16**:1289–1296. https://doi.org/10.1038/s41592-019-0619-0
26. Street K, Risso D, Fletcher RB, Das D, Ngai J, Yosef N, *et al.* Slingshot: cell lineage and pseudotime inference for single-cell transcriptomics. *BMC Genomics* 2018;**19**:477. https://doi.org/10.1186/s12864-018-4772-0
27. Jones GT, Bown MJ, Gretarsdottir S, Romaine SP, Helgadottir A, Yu G, *et al.* A sequence variant associated with sortilin-1 (SORT1) on 1p13.3 is independently associated with abdominal aortic aneurysm. *Hum Mol Genet* 2013;**22**:2941–2947. https://doi.org/10.1093/hmg/ddt141
28. Coulthard LR, White DE, Jones DL, McDermott MF, Burchill SA. P38(MAPK): stress responses from molecular mechanisms to therapeutics. *Trends Mol Med* 2009;**15**:369–379. https://doi.org/10.1016/j.molmed.2009.06.005
29. Reustle A, Torzewski M. Role of p38 MAPK in atherosclerosis and aortic valve sclerosis. *Int J Mol Sci* 2018;**19**:3761. https://doi.org/10.3390/ijms19123761
30. Aguado BA, Schuetze KB, Grim JC, Walker CJ, Cox AC, Ceccato TL, *et al.* Transcatheter aortic valve replacements alter circulating serum factors to mediate myofibroblast deactivation. *Sci Transl Med* 2019;**11**:eaav3233. https://doi.org/10.1126/scitranslmed.aav3233
31. Garoffolo G, Casaburo M, Amadeo F, Salvi M, Bernava G, Piacentini L, *et al.* Reduction of cardiac fibrosis by interference with YAP-dependent transactivation. *Circ Res* 2022;**131**:239–257. https://doi.org/10.1161/CIRCRESAHA.121.319373
32. Gao C, Hu W, Liu F, Zeng Z, Zhu Q, Fan J, *et al.* Aldo-keto reductase family 1 member B induces aortic valve calcification by activating hippo signaling in valvular interstitial cells. *J Mol Cell Cardiol* 2021;**150**:54–64. https://doi.org/10.1016/j.yjmcc.2020.10.002
33. Goettsch C, Strzelecka-Kiliszek A, Bessueille L, Quillard T, Mechtouff L, Pikula S, *et al.* TNAP as a therapeutic target for cardiovascular calcification—a discussion of its pleiotropic functions in the body. *Cardiovasc Res* 2022;**118**:84–96. https://doi.org/10.1093/cvr/cvaa299
34. Iqbal F, Lupieri A, Aikawa M, Aikawa E. Harnessing single-cell RNA sequencing to better understand how diseased cells behave the way they do in cardiovascular disease. *Arterioscler Thromb Vasc Biol* 2021;**41**:585–600. https://doi.org/10.1161/ATVBAHA.120.314776
35. Hulin A, Hortells L, Gomez-Stallons MV, O'Donnell A, Chetal K, Adam M, *et al.* Maturation of heart valve cell populations during postnatal remodeling. *Development* 2019;**146**:dev173047. https://doi.org/10.1242/dev.173047
36. Farbehi N, Patrick R, Dorison A, Xaymardan M, Janbandhu V, Wystub-Lis K, *et al.* Single-cell expression profiling reveals dynamic flux of cardiac stromal, vascular and immune cells in health and injury. *Elife* 2019;**8**:e43882. https://doi.org/10.7554/eLife.43882
37. Xu K, Xie S, Huang Y, Zhou T, Liu M, Zhu P, *et al.* Cell-type transcriptome atlas of human aortic valves reveal cell heterogeneity and endothelial to mesenchymal transition involved in calcific aortic valve disease. *Arterioscler Thromb Vasc Biol* 2020;**40**:2910–2921. https://doi.org/10.1161/ATVBAHA.120.314789
38. Decano JL, Iwamoto Y, Goto S, Lee JY, Matamalas JT, Halu A, *et al.* A disease-driver population within interstitial cells of human calcific aortic valves identified via single-cell and proteomic profiling. *Cell Rep* 2022;**39**:110685. https://doi.org/10.1016/j.celrep.2022.110685
39. Albanese I, Yu B, Al-Kindi H, Barratt B, Ott L, Al-Refai M, *et al.* Role of noncanonical Wnt signaling pathway in human aortic valve calcification. *Arterioscler Thromb Vasc Biol* 2017;**37**:543–552. https://doi.org/10.1161/ATVBAHA.116.308394